Theoretical design of high-performance polymer based magnetoelectric of fibrilar structures

C. S. Lehmann Fernandez[1], N. Pereira[1], P. Martins[1,*], S. Lanceros-Méndez[1, 2, 3]

[1] Centro de Física, Universidade do Minho, Campus de Gualtar, 4710-057 Braga, Portugal.

[2] BCMaterials, Parque Científico y Tecnológico de Bizkaia, 48160 Derio, Spain

[3] IKERBASQUE, Basque Foundation for Science, 48013 Bilbao, Spain

Abstract

Low-dimensional magnetoelectric (ME) materials are attracting high attention both from the scientific and technological communities due to their interesting electrical, optical and mechanical properties allied to their novel applications in micro and nano smart-devices, drug delivery platforms, heterogeneous catalysis, tissue engineering, biosensors and bio-actuators, among others. Once the low dimensionality of these materials complicate the direct measurement of their performance at a large range of magnetic fields and high filler contents, this work theoretically evaluates low dimensional ME structures from spherical to ellipsoidal and fibre-shaped. The structures are based on $CoFe_2O_4$/poly(vinylidene fluoride) composites and the simulations are performed through the finite element method (FEM).

Results for 50 wt.% $CoFe_2O_4$ content samples reveal ME coefficients of 182 V/cm at 684 Oe for the spheres and 4241 V/cm at a magnetic field of 208 Oe on the medium eccentricity (of 1200) ellipsoidal structure. These fibre shaped ellipsoids exhibit higher ME values than the spheres and the axisymmetric fibres: 1601 V/cm at 30 Oe for an ellipsoid with eccentricity of 3200. Further, the fibrilar structure strongly decreases the ME performance and operational magnetic field to 14.7 V/cm at 1.38 Oe.

These results establish the potential and limits, in terms of magnetic field and electric response, of the use of these composites and structures on technological ME device applications. Further, it demonstrates that suitable tuning of shape and dimensions allow to strongly increase ME response of the composites.

*corresponding author: pmartins@fisica.uminho.pt

Keywords: magnetoelectric, piezoelectric, magnetostrictive, finite elements method

1 Introduction

The evolution of technology increasingly demands size reduction and more accurate and powerful performance of devices [1]. The innovation in such devices is possible thanks to the investigation, optimization and production of new materials. The development of high performance smart materials is particularly important for sensors and actuators, among others [2, 3]. Multiferroics, smart materials which exhibit two or more ferroic properties, which include ferroelectricity, ferromagnetism and ferroelasticity, deserve special attention due to their attractive physical properties and large potential for technological applications. However, what makes multiferroic materials scientifically and technologically particularly interesting is not only their ability to display multiple order states but, most importantly, the cross coupling effects that can occur between these order states such as the magnetoelectric (ME) effect [4].

On a ME material, the application of a magnetic field influences the polarization of the material, and inversely, an electric field will result in a magnetization of the material. This coupling is, in some cases, such as ME composites, generated indirectly via stress/strain within the material. This ME response is often described by the ME coefficient (α_{ME}), as [5] :

$$\alpha_{ME} = \frac{\delta P}{\delta H} \qquad \text{Eq. 1}$$

where α_{ME} represents electrical polarization variation, P, induced by the application of a magnetic field, H.

Single-phase materials, in which ferromagnetism and ferroelectricity independently appear are rare [6], show low ME coupling at low temperatures and low Curie temperatures [7]. To overcome those limitations, ME composites emerge as a solution. Magnetostrictive (MS) and piezoelectric (PE) phases within a composite allow an improved ME response. A high number of applications have been developed on this principle [8], including magnetically controlled electro-optic devices, microwave phase shifters (electrically controlled), broadband magnetic field sensors and memory devices, among others. Strong efforts have been thus invested on enhancing the ME coupling to achieve higher values than those obtained by single phase materials [9].

Such ME composite materials can be ceramic-based or polymer-based materials, and although ceramic-based achieve ME coefficients up to three orders of magnitude higher than polymer-based ones, they present limitations due to reactions at the interfacial regions, high dielectric losses and low stability on device applications [5, 10]. Polymer-based ME materials overthrow this difficulties, with strong strain coupling, flexibility with low leakage currents, shaping feasibility, low temperature fabrication and low cost, obtaining for those features high industry interest [11].

Regarding structure, fibrilar and sphere structures present several advantages for specific applications due to larger area to volume ratio, when compared to traditional structures, such as nanocomposites and laminates [12]. Further, they show unusual electrical, optical and mechanical properties [13, 14] and, when biocompatible, fund application in biomedical applications such as drug delivery platforms, tissue engineering, biosensors and bioctuators [15-17].

Despite all these benefits and innovation opportunities, the specific features of fibres and spheres, typically at the micro or nanoscale, complicate the direct measurement of their performance at a large range of magnetic fields and high particle concentrations, mathematical models and simulations allowing to achieve this know-how in order to proper understand, tailor and predict composite performance and to design improved and smaller devices [18]. In fact….

This brings the attention to the integral knowledge of the functioning of such low dimensional structures, and its component materials, in order to understand their way to operate. Developing mathematical models and simulations that allow this understanding has become essential in the generation of new technologies that enable achieving smaller and enhanced dispositives [19].

In this work, a finite element method (FEM) [20] has been applied for the simulation of spherical, ellipsoidal and fibre-shaped ME structures to investigate the ME effect at the magnetostrictive-electroactive interfaces [21]. Polyvinylidene fluoride (PVDF) was selected as the piezoelectric polymer and cobalt ferrite $CoFe_2O_4$ (CFO) as the magnetostrictive counterpart. While PVDF presents an elevated piezoelectric response, large chemical and radiation resistance[22], CFO was selected due to its large magnetostriction, high Curie temperature, and chemical resistance[18, 23].

2 Theoretical simulation

2.1 Magnetoelectric model for finite element method simulations

The model is based on both, magnetostrictive and piezoelectric phases being in a stressed state on the bonded interface, such as in [18].

Briefly, the stressed stated is induced by the presence of an external magnetic field that affects the magnetostrictive phase of the composite. Coupling between the magneto-elastic-electric fields is computed in the two phases, driven by the elastic bonding.

The source of the external magnetic field are Helmholtz coils carrying DC current density (in order to supply a homogeneous magnetic field) and inducing a magnetic-mechanical-electrical coupling that is evaluated in terms of the magnetic vector potential (Ψ), magnetization (M), mechanical displacement vector (u), electric potential (ϕ) and electric polarization (P).

2.1.1 Fundamentals: Magnetic field model for magnetostatics

As the current density within the coils (J_e) is a steady current, and according to Maxwell´s equation, a magnetic field (H) will be generated, given by Ampere´s Law:

$$\nabla \times H = J_e \qquad \text{Eq. 2}$$

After the Gauss´s Law for magnetism, the magnetic flux density, B, is established by:

$$\nabla \cdot B = 0 \text{ , implying } \quad B = \nabla \times \psi \qquad \text{Eq. 3}$$

With Ψ representing the magnetic vector potential, and $\nabla \cdot$ and $\nabla \times$, the mathematical divergence and rotor operators, respectively.

Within the magnetostrictive phase, the magnetic induction (B) can be referred in terms of the applied magnetic field (H) and the magnetization (M). Because the magnetostrictive strains and magnetic permeability within the magnetostrictive phases are nonlinearly

influencing the magnetic flux density and strain as stresses, this relation is better represented by [24]:

$$H + M(H) = \frac{1}{\mu_0} B \qquad \text{Eq. 4}$$

In terms of Ampere´s Law, it can be also described by:

$$\nabla \times \left(\frac{B}{\mu_0 \mu_r} \right) = J_e \qquad \text{Eq. 5}$$

Where μ_0 represents the vacuum permeability and μ_r, the relative permeability of the material.

The nonlinear magnetization in Eq (4) will be given by a experimental *H-B* curve. Outside the magnetostrictive domain, permeability of air (μ_r=1) and PVDF ($\mu_r \cong 1$) are constant, allowing continuity magnetostatic conditions of normal components of *B* and tangential components of *H*. Symmetry exists in the magnetic field with respect to the zx, zy, and zz planes.

2.1.2 Magnetostriction model

By the relation of Becker and Döring [25-27], magnetostrictive strains along the i-th direction can be described as:

$$\lambda_i = \frac{3}{2} \lambda_S \left(\overline{m_i}^2 - \frac{1}{3} \right) = \frac{3}{2} \lambda_S \left(\left(\frac{M_i}{M_S} \right)^2 - \frac{1}{3} \right) \qquad \text{Eq. 6}$$

where λ_i represents the i-th component of the relative magnetostrictive deformation and λs is the polycrystalline magnetostriction constant. m_i is the magnetization direction cosine, which is the magnetization ratio along the i-th direction (M_i) and the saturation magnetization (M_s) of the magnetostrictive material. It referrers to the local magnetization ratio within a grain/domain with respect to the saturation magnetization [27],[24]. By the assumption that the material is sufficiently pre-stressed, where all magnetic moments are perpendicular to the direction of magnetization at the beginning of the process, the 1/3

term may be neglected. Therefore, within the sufficiently pre-stressed magnetostrictive material with no preferential crystallographic orientation, magnetostriction on every direction will be represented by:

$$\lambda_i = \frac{3}{2}\lambda_S \overline{m_i}^2 = \frac{3}{2}\lambda_S \left(\frac{M_i}{M_S} \right)^2 \qquad \text{Eq. 7}$$

2.1.3 Mechanical model for the magnetostrictive material

Non-linear magnetostriction is implemented by the introduction of a pre-strain in the magnetostrictive domain (Eq 7), and a null initial strain. By this means, the mechanical model within the magnetostrictive phase is given by a linear elastic model, described by [24]:

Strain-Displacement Equation:

$$S = \frac{1}{2}\left[(\nabla u)^T + (\nabla u) \right] \qquad \text{Eq. 8}$$

Hooke´s Law:

$$\sigma - \sigma_0 = C_E \cdot (S - S_0) \qquad \text{Eq. 9}$$

Newton´s Second Law for stationary case, motion equation:

$$\nabla \sigma = 0 \qquad \text{Eq. 10}$$

where u represents the displacement tensor, S is the strain tensor (with S_0 as the initial strain), σ is the Cauchy stress tensor (σ_0, the initial stress), and C_E is the elasticity matrix [28]. Finally, the magnetostrictive elastic model considers traction-free boundary conditions at outer surfaces and continuity equations of displacement and normal stress (perfect bonding) at all the interfaces of the structure.

2.1.4 Magnetostrictive material properties

Zhang et al. [29] investigated the effect of magnetic nanoparticles over the morphology, ferroelectric and magnetic behaviour of CFO/P(VDF-TrFE) 0-3 nanocomposites. This study implied that cobalt ferrite ($CoFe_2O_4$, CFO) nanoparticles have no preferential crystallographic orientation and that, when embedded in P(VDF-TrFE), CFO nanoparticle responses are deeply influenced by the concentration of CFO. These

properties and the CFO´s hysteresis curve - experimentally obtained- are presented in Table 2.

Table 1: Mechanical, magnetic and electrical properties of cobalt ferrite ($CoFe_2O_4$) [29]

Magnetostrictive Material Property					**CFO**
Structural	Density		**ρ**	(kg/m^3)	5300
	Young modulus		**Y**	(GPa)	1.39
	Poisson´s ratio		**ν**	1	0.37
Electrical	dielectric constant		**ε**	1	10
Magnetic	Permeability		**μ_r**	1	2
	Susceptibility		**χ**	1	0.03
	Curie Temperature		**τ**	K	Above 700
	sat. magnetization		**M_S**	(emu/gr)	59
	sat. magnetization		**M_S**	(kA/m)	312.7
	H-B curve	sat. induction	**B_s**	(kA/m)	315.3
		sat. magnetic field	**H_s**	(T)	1.8
		remanent induction	**B_r**	(kA/m)	153.5
		coercivity	**H_c**	(T)	0.2±0.012
Magnetostrictive	strain ratio		**β**	1	0.5
	Magnetostriction		**λ_S**	1	10^{-4}

2.1.5 Mechanical model for the piezoelectric material

Linear piezoelectric model is considered to be driven by the electric field, E, electric displacement, D, Cauchy stress tensor, σ, strain tensor, ε, and the remanent polarization, P_r. It is also modeled by the piezoelectric, d_{3n}, and the compliance, S_E, coefficient matrices, and the dielectric permittivity matrix, K_σ, by:

$$\varepsilon - \varepsilon_0 = S_E \cdot (\sigma - \sigma_0) + d_{3n}^T \cdot E \qquad \text{Eq. 11}$$

$$D = P_r + d_{3n} \cdot (\sigma - \sigma_0) + \kappa_\sigma \cdot E \qquad \text{Eq. 12}$$

Where the super index T denotes a transposed matrix, establishing converse piezoelectric effect. The electro-mechanical coupling is then guided by Gauss Law, t=0 (Eq 13) and Cauchy momentum equation, t=0 (Eq 14):

$$\nabla \cdot D = \rho_V \qquad \text{Eq. 13}$$

$$\nabla \cdot \sigma = f_V \qquad \text{Eq. 14}$$

Where the divergence ($\nabla \cdot$) of the electrical displacement field, D, and stress tensor, σ, are equal to the free electric charge density, ρ_V, and the volumetric pressure, f_V, (force per unit volume).

An assumption must be made, in order to obtain an electric potential (φ) on the external surface of the ME structure, in which zero charge is held within the structure (electrically floating electrode condition), therefore the local electric field strength, E, being directed by the variation of electric potential, as:

$$E = -\nabla \varphi \qquad \text{Eq. 15}$$

2.1.6 Piezoelectric material properties

Esterly [30] evaluated the mechanical properties of PVDF, which are summarized in Table 2.

Table 2: Mechanical and electrical properties of PVDF [30].

Piezoelectric Material Property				PVDF
Structural	Density	**ρ**	(kg/m^3)	1470
	Elasticity Matrix	$\mathbf{c_E}$	(GPa)	{{2.74, 5.21, 4.78, 0, 0, 0}, {5.21e, 2.36, 5.21e, 0, 0, 0}, {4.78, 5.21, 2.12, 0, 0, 0}, {0, 0, 0, 2.74, 0, 0}, {0, 0, 0, 0, 2.74, 0}, {0, 0, 0, 0, 0, 2.74}}
	Compliance Matrix	$\mathbf{c_E^{-1}}$	(1/GPa)	{0.365, - 0.192, 0.424, -0.209, -0.192, 0.472, 0, 0, 0, 0.365, 0, 0, 0, 0, 0.365, 0, 0, 0, 0, 0, 0.365}
Electrical	Coupling Matrix	**e**	(C/m^2)	{{0, 0, -4.761, 0, 0, -33.33}, {0, 0, 3.703, 0, 1.703, 0}, {1.703, 0, 0, 0, 0, 0}}
	Relative Permittivity	$\boldsymbol{\varepsilon_S}$	1	{{13, 0, 0}, {0, 13, 0}, {0, 0, 13}}

2.2 Structure geometry, symmetries and magnetic field values

3-D models for micro- and nanostructures require high discretization levels, and in order to produce a homogeneous magnetic field, coils have to be at least five times the longest dimension of the ME structure. Therefore, 3-D models require a high amount of

informatic resources and time, which can be reduced by introducing symmetry planes as can be achieved by the 2-D axisymmetric model.

Tri-dimensional (3-D) model of ME spheres allowed to validate the axisymmetric bi-dimensional model (2-D), that allowed to expand this results for ellipsoidal structures, fibres and cylindrical composites. Both models (3-D and axisymmetric 2-D) couple electric, magnetic and mechanical fields, where the external magnetic field is generated by a DC current density (J_0) running on Helmholtz coil(s). The ME structure was located on the geometrical center in order to establish a homogeneous magnetic field within it.

i. The coil-generated magnetic field magnetized the magnetostrictive material, producing nonlinear magnetostriction (obtained from the experimental *H-B* curve). Magnetostriction with no preferred crystallographic orientation was analyzed [29],[27].
ii. This magnetostriction couples via strain to the piezoelectric material. Within it, an electric polarization, perpendicular to the direction of the deformation induced by the initial strain, generates an electrical charge distribution.
iii. The magnetostrictive-piezoelectric interface was electrically grounded and the outside surface of the structure was considered as an electrically floating electrode (EFE). By the magnetoelectric coupling via strain, and in the presence of a magnetic field, an electric potential was generated between both interfaces. Considering zero net charge held on the electrode, a homogeneous electric potential is produced along the outer surface of the structure.
iv. The stationary ME coefficient (α_{ME}) of the structure (including only DC magnetic Bias) is defined by (Eq 16):

$$\alpha_{ME} = \left| \frac{\partial E}{\partial H_{AC}} \right| = \left| \frac{dE}{dH_{AC}} \right| = \left| \frac{\varphi}{\Delta r_{piezo}} \right| \qquad \text{Eq. 16}$$

where Δr_{piezo} expresses the thickness between ground and the electrode (piezoelectric thickness or mean piezoelectric thickness for some not homogeneous structures), and φ represents the electric potential.

2.2.1 The tri-dimensional model

The 3-D experiment consistes in an air box cube of width, height and length of 12.5 μm, a Helmholtz coil, placed symmetrically along a common axis, and separated by a distance equal to the radius of the coil, of 5 μm, and a rectangular transversal coil section of 0.5 μm x 0.5 μm.

Each coil carried an equal electrical current density J_0 (A/m^2) flowing in the same direction, producing a region of nearly uniform magnetic field between them. Current density was varied between 1x10^{11} A/m^2 and 1x10^{13} A/m^2, which produced a nearly homogeneous magnetic field along the x-axis between 22 and 2227 Oe, respectively. This range of current density values were set in order to obtain the range of magnetic field values in which the magnetoelectric curve of the spherical structures reaches a maximal performance.

2.2.2 The bi-dimensional axisymmetric model

Axisymmetric models are those with the presence of rotational symmetry and therefore are ideal for simulations with cylindrical symmetries, as an ellipsoidal structure or a fibre. In the particular case of the ME sphere, this symmetry might not be accurate but anyhow approximate, because of the radial polarization of the sphere, which can only be introduced as radial in cylindrical coordinates. This approximation only affects the amount of magnetostriction that would be transformed in the piezoelectric effect, establishing curves of ME performance that preserved their shape among the magnetic field $\boldsymbol{H}$.

The dimension of the air box in the 2-D axisymmetric model was a cylindre of 50 μm width and 300 μm height. The coil has a sectional area of 1μm width and 150 μm height, located 10 μm away from the axis-z, with the rotational symmetry. The coils carry an electrical current density J_0 (A/m^2), producing a region of nearly uniform magnetic field between them. Current density was varied between 1x10^7 A/m^2 and 1x10^{11} A/m^2, which produces a nearly homogeneous magnetic field along the x-axis between 0.12 and 6000 Oe, respectively. This range of current density values were set in order to obtain the range of magnetic field values in which the magnetoelectric curve of the spherical structures reaches a maximal performance.

The magnetic field distribution along the x direction is shown in Figure 1 within Table 3, where the relationship between electric current density and magnetic field in x direction is displayed, in both magnetic field units, A/m and Oe.

Table 3: Magnetic field along z-direction, Hz, (in A/m and Oe) and their relation with the current density input (J_0) in the Helmholtz coils for the 2-D axisymmetric model

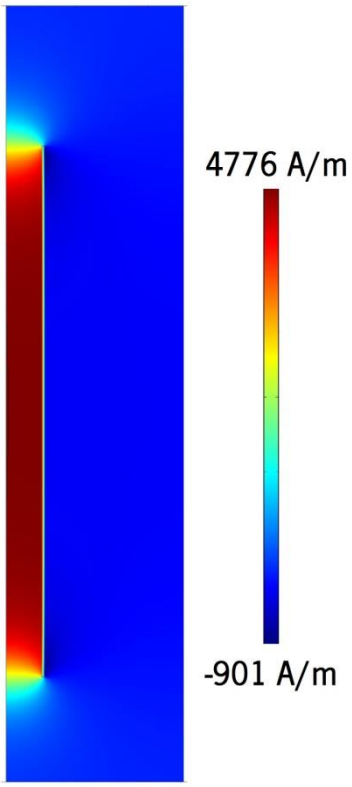

Figure 1: Distribution of the magnetic field along the z-direction, (Hz) over the axisymmetric plane when induced by one large coil.

$\mathbf{J_0}$ (A/m^2)	**Hz** (A/m)	**Hz** (Oe)
1x10^7	9.55	0.12
5x10^7	47.75	0.6
1x10^8	95.5	1.2
5x10^8	477.53	6
1x10^9	955.06	12
5x10^9	4775.29	60
1x10^{10}	9550.58	120.02
5x10^{10}	47752.89	600.08
1x10^{11}	95505.79	1200.16
5x10^{11}	477528.92	6000.8

2.2.3 Magnetoelectric structure geometry: spheres and ellipsoidal structures

The initial sphere experiment was composed by two concentrically located spheres (of radios R and r), the smallest sphere (of radius r) being the magnetostrictive CFO component and the external spherical shell (of thickness $\Delta r=R-r$) being the piezoelectric PVDF component of the spherical composite [18]. The polarization of the piezoelectric material was established radial in the boundary conditions of the problem, as the

magnetization was fixed parallel to the x-axis (in the 3-D model) and parallel to the z-axis in the 2-D axisymmetric model.

3-D ME sphere and 2-D axisymmetrical sphere and ellipsoidal ME structures presented a 50wt% concentration of CFO. The validated ME sphere was transformed into a series of ellipsoidal ME structures maintaining the volume and the concentration of the initial sphere (R=700nm and concentration of 50wt.%) but changing the ellipsoids eccentricity, **e,** until becoming approximately a fibre (images of all ellipsoidal structures are displayed in Figure 2 and sizes and concentrations, in Table 4. For symmetry reasons, the ellipsoids must be also axisymmetric and therefore, they are only defined by one major axis (***a***) and one minor axis (***b***). The ME structure was composed by two ellipsoids: the internal (magnetostrictive ellipsoid) and the external (piezoelectric) ellipsoid, both holding the same eccentricity value. In order to simplify the calculation of the ME coefficient, the piezoelectric thickness (that was not constant over the structure) has to be considered as the simple subtraction of the external and internal ellipsoids minor axis ($\Delta r = a_{piezo} - a_{ms}$). All sizes values are presented in Table 4.

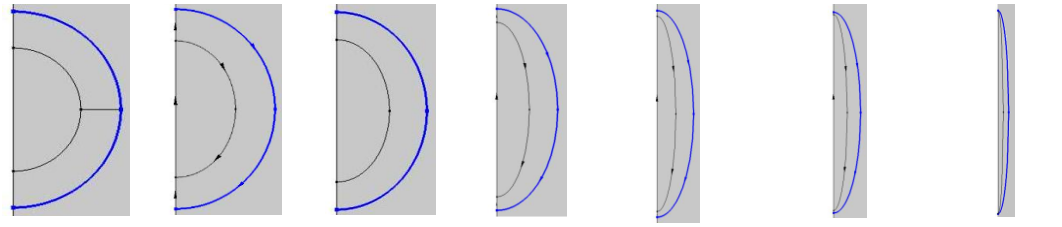

e (nm)	e (nm)	e (nm)	e (nm)	e (nm)	e (nm)	e (nm)
0	300	400	800	1200	1600	3200

Figure 2: Representation of the sphere and the ellipsoids according to their excentricity: whereas the excentricity of 0 represents the axisymmetric ME sphere, the ellipsoid with excentricity of 3200 nm can be considered as a fibre

Table 4: Ellipsoids geometrical major and minor axis as function of its eccentricity (e) for every simulation experiment, together with the corresponding values of weight concentration of cobalt ferrite (wt.%), total volume (total volume, constant value), magnetostrictive internal ellipsoid parameters (magnetostrictive ellipsoid (ms ellip.): major axis a_{CFO}, minor axis b_{CFO}) and

piezoelectric external ellipsoidal parameters, (piezoelectric ellipsoid (pzo ellip.): major axis a_{pzo}, minor axis b_{pzo}, piezoelectric thickness $\Delta r = b_{pzo} - b_{CFO}$).

e (nm)	total vol. $(\mu m)^3$	pzo ellip. a_{PZO} (nm)	pzo ellip. b_{PZO} (nm)	ms ellip. a_{CFO} (nm)	ms ellip. b_{CFO} (nm)	Δr (nm) $b_{PZO} - b_{CFO}$
0	1.44	700	700	440	440	260
300	1.44	743	680	508	410	270
400	1.44	776	665	559	390	275
800	1.44	993	588	860	315	273
1200	1.44	1300	512	1230	263	249
1600	1.44	1660	454	1620	230	224
3200	1.44	3216	326	3204	163	163

2.2.4 Magnetoelectric axisymmetric fibre model

The magnetostrictive cylinder was designed with a total length of 25 μm and was divided into two symmetrical cylinders of 12.5 μm length each, in order to establish symmetry in the centre of the fibre with respect of the z-axis (therefore reducing computer resources). The piezoelectric shell was located in the middle of the magnetostrictive rod (therefore preserving the symmetry with respect to the z-axis), with a height of 12.5 μm. The polarization of the piezoelectric material was established as radial in the boundary conditions of the problem, as the magnetization was fixed parallel to the z-axis. For the fibre ME structures, the study focuses in analysing the influence of size and concentration of the composite over the ME coefficient. ME structures of diameters of 1.4, 0.6 and 0.1 μm were analysed for concentrations of 90, 50 and 10 wt.% of CFO, with no preferred crystallographic orientation. The relationship between concentration (wt.%), sphere radius (R), magnetostrictive radius (r) and piezoelectric thickness (Δr) for all simulations is established in Table 5.

Table 5: Sphere geometrical conditions according to the concentration (wt.%) of cobalt ferrite ($CoFe_2O_4$, CFO): the external sphere radius (R), the internal magnetostrictive sphere radius (ms radius, r) and the piezoelectric thickness (pzo thickness, Δr).

concentration (wt. %)	fibre radius (r, nm)	ms radius (r, nm)	pzo thickness (Δr, nm)
10	700	105	595
50	700	242	458
90	700	429	271

50	300	103	197
50	50	17	33

2.2.5 Magnetoelectric fibre-shaped composite

In order to be compared with the cylindrical fibre, the model was established to preserve the external diameter of the ME fibre of 1.4 μm and 50 wt.% of weight concentration. The major difference is the shape of the magnetostrictive component, which was included in the present model as a specific number of CFO micro spheres embedded in a cylindrical PVDF matrix, as presented in Figure 3.

Figure 3: Tri-dimensional (3-D) view of the cylindrical (fibre-formed) micro-composite ME structure simulation.

In the centre of the piezoelectric cylinder, 38 spherical spheres of CFO with 325 nm of radius were distributed in the z-axis with a separation d_{sp} between each other. Simulations were performed for no preferential crystallographic orientation and for spheres separations, d_{sp}, of 4 nm and 7 nm.

3 Results and Discussion

The validation of the 2-D axisymmetrical model with the 3-D model is first presented in order to develop a fibre structure from the 2-D axisymmetric sphere. As the magnetic component of the problem shows complete axisymmetry, the characteristic ME response over magnetic field maintaines their shape in both 3-D and 2-D models, holding a maximal performance around 700 Oe, as presented in **Erro! A origem da referência não foi encontrada.**.

The main difference between the two sphere models is presented by the polarization on the polymer, which is radial for the 3-D model and radial in cylindrical coordinates for

the axisymmetrical model. This means, that in the axisymmetrical model there should be maximal polarization for z=0, and minimal near the symmetrical axis, where the maximal deformation should be produced in the magnetostrictive part of the structure. This difference has a direct impact in the quantitative differences obtained for the ME coefficients, showing lower values for the axisymmetrical model than for the 3-D model. This effect can be observed in **Erro! A origem da referência não foi encontrada.** (a), where the 3-D and 2-D ME coefficient for the axisymmetric models for a sphere of diameter 1.4 μm and 50 wt.% CFO are presented.

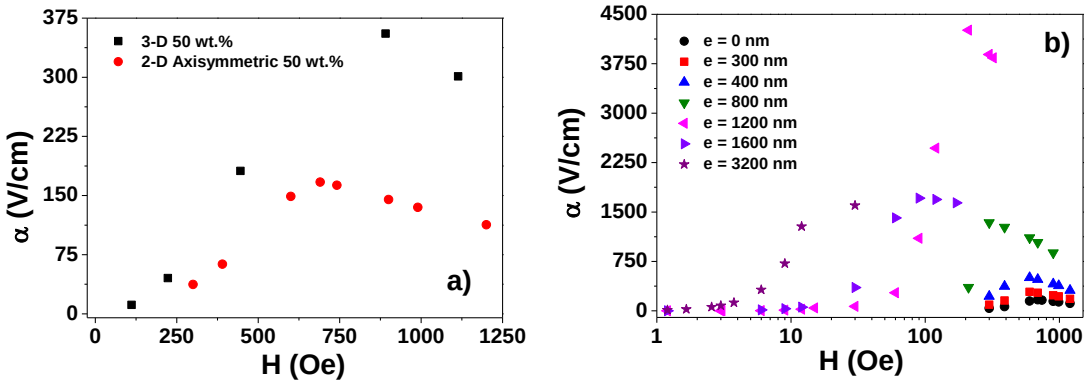

Figure 4: (a) Comparison of the α_{ME} dependence with the applied magnetic field of a 1.4 μm diameter magnetoelectric sphere for CFO concentrations of 50wt.% when modeled by the 2-D axisymmetric model and 3-D model (right). (b) ME coefficient for 50wt.% CFO content structures with different ellipsoidal eccentricities at constant volume.

As magnetostriction induces a relative deformation to the initial length of the structure, mainly along the direction of the magnetic field, it can be expected that stretching the geometry of the ME sphere into an ellipsoid with the major axis along the magnetic field direction will increase the ME response of the structure. Beside this, by increasing the area of the structure that is normal to the magnetic field, it can be also expected that the magnetization will reach higher values inside the magnetostrictive component with lower magnetic field values, giving as a result that the eccentricity of the ellipsoidal shape of the ME sphere also displaces the ME curve to the left, presenting maximal behaviour with lower magnetic fields. This effect is shown in Figure 4 (b), where simulation results for the ME performance are presented for ME structures with eccentricities between 0 nm (sphere) and 3200 nm (fibre-shaped). The concentration and total volume of the ME

structures are preserved as the ones for the sphere with diameter of 1.4 μm and 50wt.% filler content.

Figure 4b shows increasing eccentricity up to 1200 nm enhances the ME performance, while the maximal operational magnetic field diminishes. The ME structure with eccentricity of 1200 nm shows the highest ME performance, reaching more than ten times the α_{ME} of the ME sphere. Table 6 shows the maximal operational magnetic field value and maximal ME coefficient, α_{ME}, for each configuration, according to their eccentricities.

Table 6: Maximal operational magnetic field value and maximal magnetoelectric coefficient for each investigated configuration, according to their eccentricities

Configuration eccentricity *e* (nm)	**Maximal operational magnetic field H_{max} (Oe)**	**Maximal ME coefficient α_{ME} (V/cm)**
0 (3-D model)	445-890	355
0	684	182
300	611	290
400	588	508
800	298	1338
1200	208	4241
1600	90	1709
3200	30	1601

Further increasing the structure eccentricity, maximal operational magnetic fields continues to reduce, and the curves return to a smoother shape, but reducing gradually their ME performance and showing for fibre-shaped structures a monotone increasing curve (as presented for the configuration with eccentricity of 3200 nm).

According to those arguments, three-types of ellipsoidal-shaped ME structures can be established. The first type are the ellipsoidal-spherical ME structures, with eccentricities bellow 800 nm that operate in DC magnetic fields between 200-2000 Oe, with simulated α_{ME} of the order of hundreds and with a ME curve with a similar shape as a spherical structure. The second type of ellipsoidal structures show a giant ME effect and are the ones with eccentricities above 800 nm and below 1600 nm. They show a more abrupt curve and operate between 20 and 200 Oe magnetic DC bias field. It should be noticed the existence of an exceptional ME behaviour of the ME structure of eccentricity of 1200 nm, with a ME coefficient of the order of 4000V/cm. The third type is the fibre type. These are structures with eccentricities above 1600 nm, show a lower order of magnitude of α_{ME} than the second group and operate at very low DC bias fields, below 20 Oe.

Erro! A origem da referência não foi encontrada. shows the normal magnetic flux density distribution for ellipsoidal ME structures of the third group, when exposed to a magnetic field of 12 Oe.

H_z	12 (Oe)	12 (Oe)	12 (Oe)	Scale
MAGNETIC FLUX DENSITY NORM (B_{NORM})	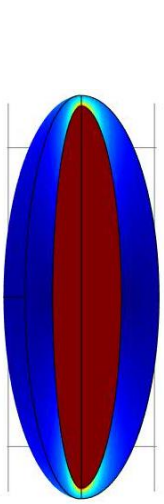	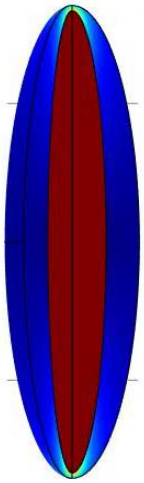	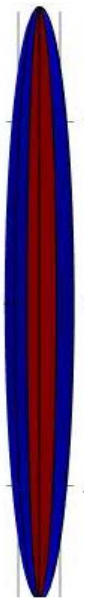	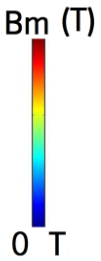
MAX	0.02 T	0.035 T	0.17 T	**Bm**
e	1200 nm	1600 nm	3200 nm	**e**

Figure 5: Normal magnetic flux density of the more eccentric magnetoelectric ellipsoidal structures when a magnetic field of 12 Oe (in z-direction) is applied.

As expected, with increasing the eccentricity of the fibre-shaped structures, magnetization saturation is reached at lower magnetic fields, therefore, showing a higher and more homogeneous normal magnetic flux density at lower magnetic fields, as shown in **Erro! A origem da referência não foi encontrada.**.

The second group of ME ellipsoidal structures show the highest ME performance and a very interesting new area that should be followed by further research. The elaboration of ME structures with such specific geometrical conditions is typically limited and therefore these experiments are carried out just in order to present tendencies of ME performances related to geometry optimization. The main objective of this experiment was to obtain the trends of the ME curves and maximal operational magnetic field of ME fibres, therefore establishing the pattern to expect for the fibre simulations, i.e. lower operational magnetic fields, defined by the normal area to the magnetization direction of the fibre, which is larger than the sphere.

3.1 2-D Axisymmetric fibre simulations

The former ellipsoidal ME structures simulations established that increasing the magnetostrictive surface perpendicular to the magnetization leads to a decrease of the magnetic field for maximal α_{ME}, (H_{max}). Therefore, and as all fibres have the same length, this surface depends only on the magnetostrictive rod radius, which increases with the diameter of the fibre and with the content of CFO. Figure 6 shows this effect, presenting α_{ME} values for CFO/PVDF fibres with different CFO content (10 wt.%, 50 wt.% and 90 wt.% with 1.4 µm of diameter) and different sizes (0.1 µm, 0.6 µm and 1.4 µm of diameter and 50 wt.% CFO content).

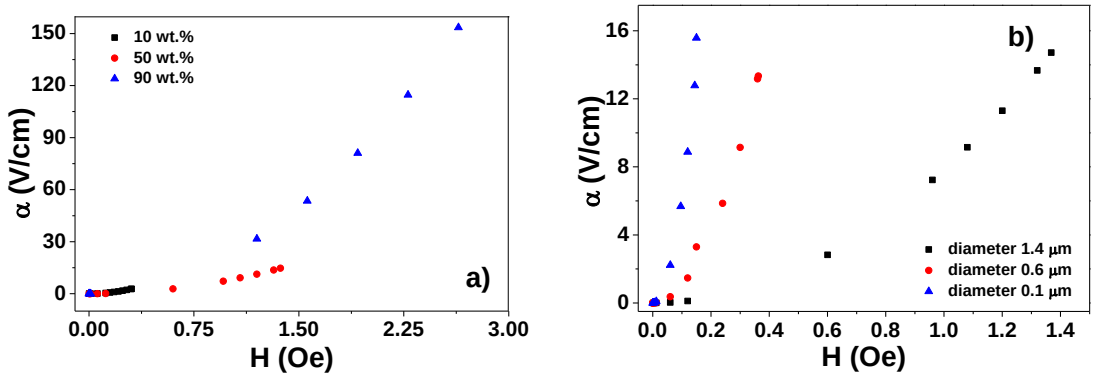

Figure 6: Simulations results for magnetoelectric performance of fibre structures of (a) 1.4 µm diameter, with 10wt.%, 50wt.% and 90wt.% content of CFO and (b) 50wt.% ME fibres with diameters of 0.1 µm, 0.6 µm and 1.4 µm.

A strong effect can be observed in the ME coefficient when diminishing its CFO content, establishing higher ME performance with higher CFO content, reaching values of 10 times higher α_{ME} for 90 wt.% fibres than for 50 wt.%, and presenting different operational magnetic fields, as presented in Table 7. Clear trends are presented with the operational magnetic field increasing with fibre diameter and magnetostrictive content, while the size of the fibre allows to tune the operational magnetic field: lower operational magnetic fields being obtained for smaller fibre diameters.

Table 7: Maximal operational magnetic fields and maximum magnetoelectric coefficient as a function of fibre diameter and filler content.

wt.% CFO	Fibre diamter (µm)	Maximal operational magnetic field	Maximal ME coefficient

		H_{max} (Oe)	α_{ME} (V/cm)
50	0.1	0.15	15.58
50	0.6	0.36	13.34
10	1.4	0.3	3.2
50	1.4	1.38	14.7
90	1.4	2.63	153

3.2 2-D Axisymmetric cylindrical micro-composite simulations

Finally, the last set of experiments gathers all former experiments into one. It consists on multiple magnetostrictive spheres located in the middle of a cylindrical piezoelectric shaped structure, with the generation of a cylindrical ME composite. The concentration was maintained at 50 wt.%, as for former experiments, and the separation between spheres was evaluated. Figure 7 presents the ME performance for composites with 4 nm and 7 nm of separation of the magnetostrictive spheres located in the cylindrical ME composite, respectively.

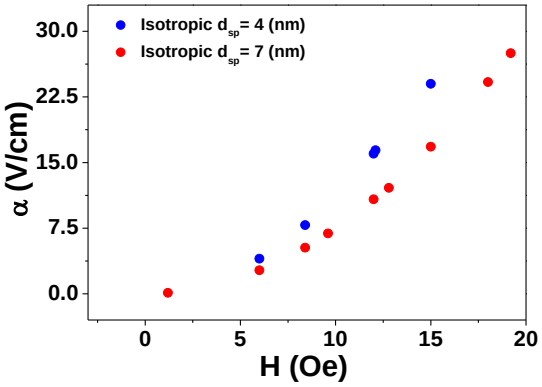

Figure 7: Magnetoelectric performance of two CFO/PVDF cylindrical composites with 50 wt.% filler content with two different separations between the CFO spheres: of 4 nm and 7 nm.

Results show that closely located ME CFO spheres embedded into a PVDF polymer matrix preserves the trend of the fibre, but increases not only the ME performance, but also the operational magnetic fields, as can be observed in Figure 7. The range of operational magnetic fields that the composite reaches is much higher than the one obtained for the fibre, but lower than the one simulated for the ellipsoidal ME structure. Also, the ME coefficients are higher but in the order of those obtained for the fibers, and much lower than those obtained for the ellipsoidal structures

(of about 24 to 27.5 V/cm, for the lower and higher separated magnetostrictive spheres structures, respectively), as shown in Table 8.

Table 8: Maximum operational magnetic field value and maximum magnetoelectric coefficient for different micro structures. CFO filler content 50 wt.% .

Structure	**Diameter (μm)**	**Maximal operational magnetic field H_{max} (Oe)**	**Maximal ME coefficient α_{ME} (V/cm)**
sphere 2-D Axisymmetric	1.4	684	182
ellipsoidal e=3200nm	0.652	30	1601
fibre	1.4	1.38	14.7
cylindrical composite d_{SP} 4nm	1.4	15	24
cylindrical composite d_{SP} 7nm	1.4	19	27.5

Figure 8 shows the ME response of the CFO/PVDF composite when subjected to a magnetic field of 12 Oe, with the electric potential distribution in a rotated 3-D way -Figure 8(a)-, with the total displacement within structure -Figure 8(b)-, the normal magnetic flux density -Figure 8(c)- and the electric potential on the piezoelectric matrix -Figure 8(d)-. Here the fibre areas display the magnetization in the axis direction (z) and the arrows display the polarization of the piezoelectric material.

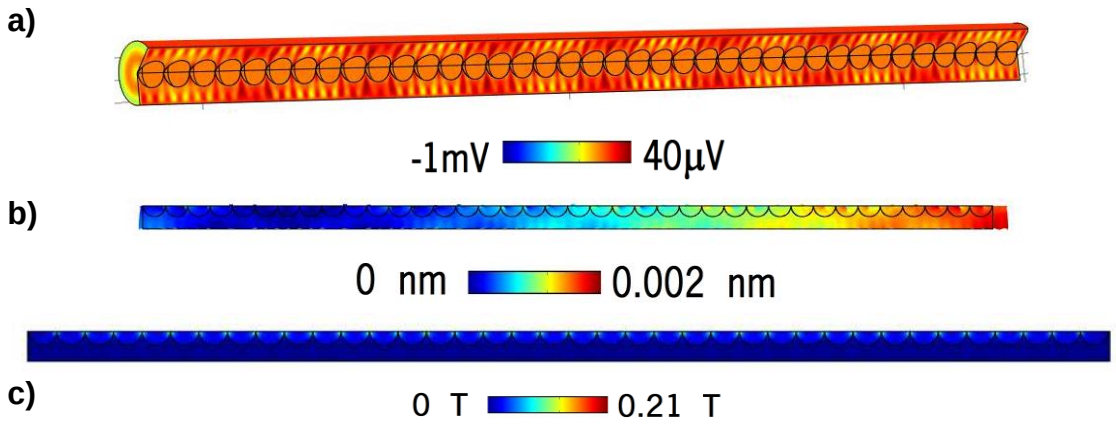

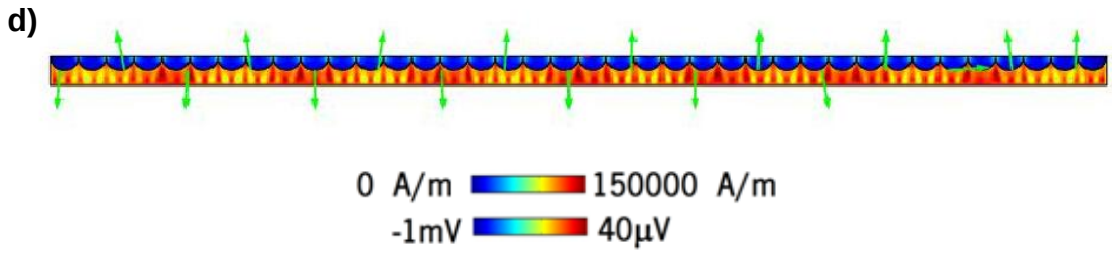

Figure 8: Magnetoelectric performance of the CFO/PVDF composite when subjected to a magnetic field of 12 Oe. (a) Electric potential distribution in a rotated 3-D way, (b) deformation of the structure, (c) normal magnetic flux density and (d) electric potential on the piezoelectric matrix. The magnetostrictive areas display the magnetization in the axis direction (z) and the arrows display the polarization of the piezoelectric material.

Figure 8 show that the electric potential distribution generates a radial pattern within the PVDF with maximum and minimum values along the z-axis, which are produced by the compressions and tensions by the displacements of the magnetostrictive structures along this direction. Normal magnetic flux density shows a nearly homogeneous distribution, with the exception of the areas between the magnetostrictive spheres, that provide for the maximal values and therefore, it can be established that the distance between them is the main component that will determinate the magnetic behaviour of the composite.

Closely located magnetostrictive spheres embedded into a PVDF matrix, lead to a larger magnetic similitude to a fibre than to a number of ME spheres, acting independently on the ME composite. The operational magnetic fields of the structures show that it behaves closer to a ME ellipsoidal structure than to a fibre. The distance between the magnetostrictive spheres allows the magnetic field to interact with the lateral surfaces, and therefore with a more perpendicular surface than a sphere alone (as the ellipsoidal ME structure), but less normal surface than a cylinder (that would have all surface perpendicular to the magnetic field). For this reason, increasing the distance of the magnetostrictive spheres allows them to interact more independently with the piezoelectric material, leading to a better magnetoelectric performance, at higher magnetic fields.

4 Conclusions

ME sphere and fibre composites, based on magnetoestrictive spheres (CFO) and a piezoelectric polymer (PVDF) were simulated by finite element method.

A 3-D and a 2D-axisymmetrical model were used to simulate the ME performance CFO/PVDF spheres of 1.4 μm diameter and 50 wt.% filler content. Taking into account the approximations used to simplify the 3-D model into a 2-D axisymmetric model, a good agreement in the ME curve over the applied magnetic field was found.

Ellipsoidal shaped ME spheres were analysed, stretching their shape and therefore increasing their eccentricity. Results allow to establish that when more normal surface of the magnetostrictive structure is exposed to a magnetic field, lower value of magnetic fields are required to increase magnetization and, therefore, smaller magnetic field values for optimal ME coefficient are needed for more eccentrically ellipsoids and fibres. Even more, three particular groups of ME structures are distinguished according to this argument:

i. Spheres (or ellipsoids with low eccentricity) that operate in higher ME fields (200-2000 Oe) show a high ME performance. By increasing their eccentricity, the ME coefficients increase leading also to lower operational magnetic fields.
ii. Medium eccentricity ellipsoidal ME structures, with the highest ME performance, present giant ME and operational magnetic fields 20-200 Oe.
iii. Fibre-shaped ellipsoids operate below 20 Oe and reveal the lowest ME performances.

The ME coefficient for the for the sphere with 50 wt.% filler content was 182 V/cm at 684 Oe, the medium eccentricity ellipsoidal structure (with eccentricity of 1200) enhanced more than ten times this result, with 4241 V/cm at a magnetic field of 208 Oe. Fibre shaped ellipsoids show higher ME values than the sphere and the axisymmetric fibre: 1601 V/cm at 30 Oe for an ellipsoid with eccentricity of 3200. The axisymmetric fibre, decreases the ME performance and operational magnetic field to 14.7 V/cm at 1.38 Oe.

Finally, the analysis of the cylindrical composite where CFO spheres were embedded into a PVDF matrix, led to conclude that the separation of the spheres will determine whether the composed structure will behave as a single structure or as multiple spheres, obtaining higher ME performance at higher magnetic fields when the separation of the spheres is increased. Thus, a value of 27.7 V/cm at 19 Oe is obtained for the case of separation

between CFO spheres of 7 nm and 24V/cm at 15 Oe for the experiment with 4 nm separation between CFO spheres.

Thus, it is demonstrated that novel ME structures can be designed with optimized shapes and response for specific applications.

Acknowledgements

The authors thank the Erasmus Mundus VECCEU scholarship and FCT- Fundação para a Ciência e Tecnologia- for financial support in the framework of the Strategic Funding UID/FIS/04650/2013 and under project PTDC/EEI-SII/5582/2014. P. Martins acknowledges also support from FCT SFRH/BPD/96227/2013 grant. The authors acknowledges funding by the Spanish Ministry of Economy and Competitiveness (MINECO) through the project MAT2016-76039-C4-3-R (AEI/FEDER, UE) (including the FEDER financial support). Financial support from the Basque Government Industry Department under the ELKARTEK program is also acknowledged.

REFERENCES

1. Bruchhaus, L., et al., *Comparison of technologies for nano device prototyping with a special focus on ion beams: A review.* Applied Physics Reviews, 2017. **4**(1).
2. Surowiak, Z. and D. Bochenek, *Multiferroic materials for sensors, transducers and memory devices (review article).* Archives of Acoustics, 2008. **33**(2): p. 243-260.
3. Wang, X., J. Sparkman, and J. Gou, *Electrical actuation and shape memory behavior of polyurethane composites incorporated with printed carbon nanotube layers.* Composites Science and Technology, 2017. **141**: p. 8-15.
4. Vopson, M.M., *Fundamentals of multiferroic materials and their possible applications.* Critical Reviews in Solid State and Materials Sciences, 2015. **40**(4): p. 223-250.
5. Martins, P. and S. Lanceros-Méndez, *Polymer-Based Magnetoelectric Materials.* Advanced Functional Materials, 2013. **23**(27): p. 3371-3385.
6. Eerenstein, W., N.D. Mathur, and J.F. Scott, *Multiferroic and magnetoelectric materials.* Nature, 2006. **442**(7104): p. 759-65.
7. Pan, D.A., et al., *Shape and size effects on layered Ni/PZT/Ni composites magnetoelectric performance.* Journal of Physics D: Applied Physics, 2008. **41**(17): p. 172003.

8. Fuentes, M.E., et al., *Meso- and nano- magnetoelectricity: a review.* Revista mexicana de física, 2007. **53**: p. 21-29.
9. Lupascu, D.C., et al., *Measuring the magnetoelectric effect across scales.* GAMM-Mitteilungen, 2015. **38**(1): p. 25-74.
10. Sun, K.H., et al., *Optimal configuration of magnetoelectric composites under various mechanical boundary conditions.* Composites Science and Technology, 2017. **142**: p. 221-226.
11. Maceiras, A., et al., *High-temperature polymer based magnetoelectric nanocomposites.* European Polymer Journal, 2015. **64**: p. 224-228.
12. Jin, J., et al., *Multiferroic Polymer Composites with Greatly Enhanced Magnetoelectric Effect under a Low Magnetic Bias.* Advanced Materials, 2011. **23**(33): p. 3853-3858.
13. Arico, A.S., et al., *Nanostructured materials for advanced energy conversion and storage devices.* Nat Mater, 2005. **4**(5): p. 366-377.
14. Ge, M., et al., *A review of one-dimensional TiO2 nanostructured materials for environmental and energy applications.* Journal of Materials Chemistry A, 2016.
15. Otaigbe, J.U., et al., *Generation, Characterization, and Modeling of Polymer Micro- and Nano-Particles*, in *Polymer Physics and Engineering*. 2001, Springer Berlin Heidelberg: Berlin, Heidelberg. p. 1-86.
16. Luo, C.J., et al., *Preparation of polymeric nanoparticles by novel electrospray nanoprecipitation.* Polymer International, 2015. **64**(2): p. 183-187.
17. Ribeiro, C., et al., *Proving the suitability of magnetoelectric stimuli for tissue engineering applications.* Colloids and Surfaces B: Biointerfaces, 2016. **140**: p. 430-436.
18. Lehmann Fernández, C.S., et al., *Evaluation and optimization of the magnetoelectric response of CoFe<inf>2</inf>O<inf>4</inf>/poly(vinylidene fluoride) composite spheres by computer simulation.* Composites Science and Technology, 2017. **146**: p. 119-130.
19. Tan, X. and J.S. Baras, *Adaptive identification and control of hysteresis in smart materials.* IEEE Transactions on Automatic Control, 2005. **50**(6): p. 827-839.
20. Daelemans, L., et al., *Finite element simulation of the woven geometry and mechanical behaviour of a 3D woven dry fabric under tensile and shear loading using the digital element method.* Composites Science and Technology, 2016. **137**: p. 177-187.
21. Gonçalves, R., et al., *Development of magnetoelectric CoFe2O4 /poly(vinylidene fluoride) microspheres.* RSC Advances, 2015. **5**(45): p. 35852-35857.
22. Singh, H.H., S. Singh, and N. Khare, *Design of flexible PVDF/NaNbO<inf>3</inf>/RGO nanogenerator and understanding the role of nanofillers in the output voltage signal.* Composites Science and Technology, 2017. **149**: p. 127-133.
23. Della Pina, C., et al., *A green approach to magnetically-hard electrically-conducting polyaniline/CoFe<inf>2</inf>O<inf>4</inf> nanocomposites.* Composites Science and Technology, 2015. **110**: p. 138-144.
24. Zadov, B., et al., *Modeling of small DC magnetic field response in trilayer magnetoelectric laminate composites.* Advances in Condensed Matter Physics, 2012. **2012**.
25. Bozorth, R.M., *Ferromagnetism*. 1951, New York: Van Nostrand.
26. Chikazumi, S. and C.D. Graham, *Physics of Ferromagnetism*. 1997: Clarendon Press.
27. Hao Xu, Y.P., Daining Fang, Shigang Ai, *An energy-based dynamic loss hysteresis model for giant magnetostrictive materials.* International Journal of Solids and Structures, 2013. **50**(5): p. 672-679.
28. Graham, F., *Development and validation of a bidirectionally coupled magnetoelastic FEM model for current driven magnetostrictive devices*, 2009, University of Maryland, College Park: Ann Arbor. p. 144.
29. Zhang, J.X., et al., *The effect of magnetic nanoparticles on the morphology, ferroelectric, and magnetoelectric behaviors of CFO/P(VDF-TrFE) 0–3 nanocomposites.* Journal of Applied Physics, 2009. **105**(5): p. 054102-054102.

30. Esterly, D.M., *Manufacturing of Poly (vinylidene fluoride) and Evaluation of its Mechanical Properties*, 2002. p. 1-55.